DOE/ER/60233--T8

DOE GRANT # DE FG03-84ER60233

DOE ANNUAL REPORT

1994-95

DISCLAIMER

DISCLAIMER

Portions of this document may be illegible electronic image products. Images are produced from the best available original document.

PROGRESS REPORT

The published work in the accompanying references details much of the work in our List of Accomplishments and should be self-explanatory. Here we describe results which have not yet been published.

Studies of Biologic Activation Associated with Molecular Receptor Increase and Tumor Response in ChL6/L6 Protocol Patients

Several patients in these studies had superficial tumors which developed evidence for inflammatory reactions manifested by warmth, erythema, and/or tenderness within a few hours of infusion of unlabeled antibody. These findings led to a study of several parameters of biologic systems activation associated with ^{131}I ChL6 treatment. Complement activation, ADCC enhancement of NK and monocyte/macrophage PBMN's, IL-1, IL-2, and IL-2 receptor (IL-2R) levels in serum, serum albumin, tumor uptake and radiation dose were examined to evaluate the role of synergy between the biologic systems and the radiation leading to therapeutic responses. In the first 10 therapy patients, C3, C4 and albumin levels fell during both L6 and ChL6 infusions and remained below normal for hours to days post therapy. Patients in the antibody dose escalation study receiving preload doses of 50, 100, 150, or 200 mg of L6 did not demonstrate a significant increase in their IL-2 receptor level unless 150 mg or more had been given. The first 9 patients receiving imaging and therapy infusions on sequential days demonstrated a dose and time dependent increase of soluble IL-2 receptor levels in serum when compared to preinfusion baseline levels. In 2 patients, IL-2 levels were elevated shortly after initiation of the infusion of L6 or ChL6. IL-2 levels, however, could not be detected by the assay once the IL-2 receptor level had risen. Levels of IL-1α varied in the 9 therapy patients and many decreased after the initial 200 mg of L6 or ChL6 (108,109). The dosimetry from the studies suggests that there may well be synergy of tumor cell kill from the effects of combined low level irradiation with biologically triggered molecular events in the cell. These effects will be further investigated in the molecular biology studies proposed for the next grant period.

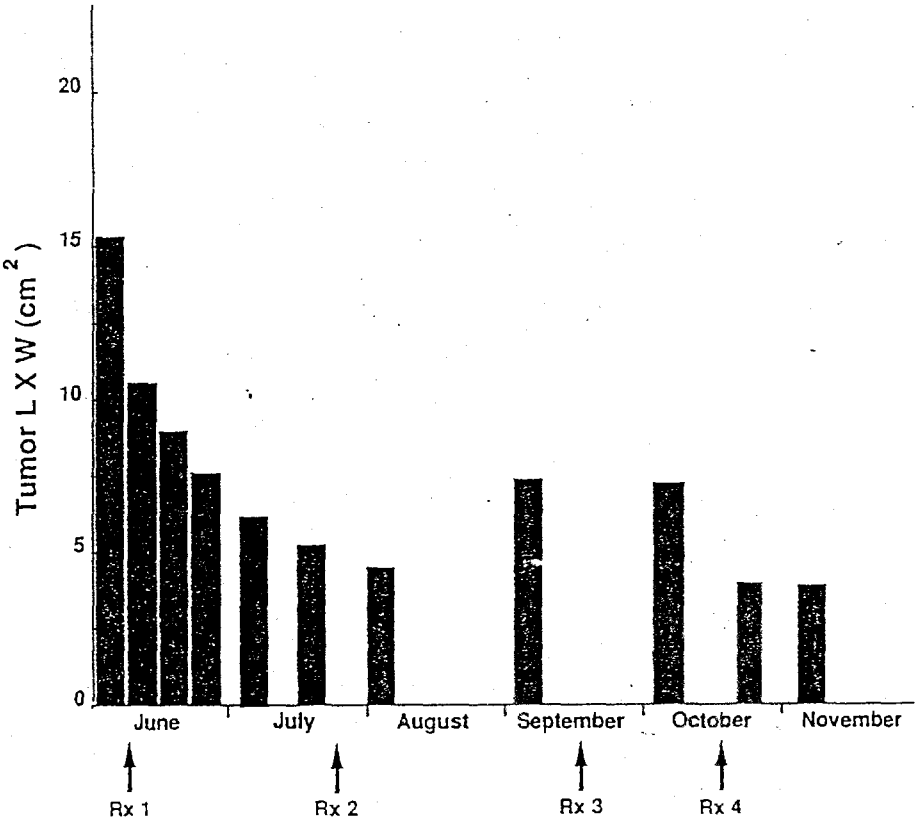

Figure 8. Therapy course of a patient demonstrating regression of her tumor in response to ^{131}I ChL6 therapy doses (Rx 1-4). All measurable tumor areas are graphically shown as the sum of the products of their longest diameter and the greatest perpendicular diameter obtained from caliper measurements taken by two physicians before therapy and at frequent intervals after each of her therapy doses.

In conclusion, these findings suggest that the biologic activity of L6 and ChL6 in vivo was responsible for enhanced tumor uptake of ^{131}I ChL6 in many of our patients secondary to transient, increased vascular permeability without significant adverse clinical sequelae. Complement activation and IL-2 receptor release may have been triggered by separate mechanisms. Tumor response was seen more frequently in this study than in any previously reported study using radioimmunoconjugates in solid tumors (Figure 8). Because of the correlation of IL-2R rise to the tumor response and relatively modest radiation doses in several responding tumors, we postulate that responses may have been secondary to synergy between enhanced delivery of the targeted radiation and sensitizing effects on tumor caused by activated effector cell mechanisms. Clinical studies of L6 and ChL6 alone had minimal to no therapeutic response (110-112).

Lym-1 Single Chain Genetically Engineered Molecules

Lym-1 recognizes a cell membrane-located antigen on human lymphoma cells that has a molecular weight of 31-35 kD and is not shed or modulated (113). Lym-1 is highly B cell specific cross reacting only slightly with surface epithelial cells of the colon and macrophages of the skin; it reacts preferentially with malignant B cells. Lym-1 does not react with normal or malignant T cells, but does react with a broad range of B tumor cell lines, 40% of specimens from patients with B cell chronic lymphocytic leukemia and at least 80% of specimens from patients with B cell lymphoma (113). The number of binding sites per Raji B lymphoma cell was found to be $1x10^6$ and the avidity constant was found to be $4x10^8$ M^{-1} for Lym-1 (113).

In the low fractionated ^{131}I-Lym-1 therapy study initiated as a patient feasibility study under this grant, 17 of 30 of Lym-1 reactive patients had durable responses (114). In the maximum tolerated dose ^{131}I-Lym-1 study, 13 of 24 patients had durable responses including 8 complete remissions (115). The radiation dose-limiting toxicity was thrombocytopenia (116). Others have confirmed the responsiveness of patients with hematopoietic malignancies using this agent (117), and other radiolabeled antibodies alone (118-123) and in association with bone marrow transplantation (124). While these trials proved successful, they also demonstrated the need to enhance the conditions for treatment in order to more generally achieve longer remissions or cure.

The first step in the production of the gene expressing the Lym-1 SCA was sequencing of the mRNA from the hybridoma cell encoding the murine monoclonal antibody Lym-1. Primers were then designed to convert the mRNAs encoding the heavy and light chains to cDNAs. A second set of primers were designed to use in Polymerase Chain Reaction amplification of the cDNA. The primers also incorporated restriction enzyme endonuclease cleavage sites at the ends of these stretches to use for the ligations to assemble the gene. The encoding of the segment linker peptide was prepared from two single stranded lengths of synthesized DNA, which were annealed and converted to double stranded DNA, and also cut with restriction enzymes so that they could be ligated between the 3' end of the light chain F_v gene and the 5' end of the heavy chain F_v gene. A hybrid operator/promoter site was produced in a similar fashion. The gene was cut at the ends with restriction endonucleases *EcoRI* and *BamHI* and put into plasmid pUC8 for transformation of the hosts. The *E. coli* hosts initially used to express this protein have the cI857 temperature sensitive lambda repressor mutation so that they can be grown at 29° C, and then protein expression induced by raising the temperature to 42° C. Several variations of this SCA have been produced and are currently being purified for further evaluation.

Analysis of Molecular Genetic Coded Messages to Enhance Tumor Response

In order to consider other agents or targets for molecular triggers which may enhance the sensitivity of the tumor cell by enhancing death when combined with low dose rate radiation delivered by targeted therapy, selected genetic expression profiles are being studied in nude mouse human tumor xenograph models. Expression of apoptosis-associated ($TGF\beta_1$, p53 TNF), cytokine (IL-6, IL-2, IL-2R) and prognosis-associated (NM23-HI, MDR-1) genes will be monitored in studies planned to determine the LD_{50} of ^{90}Y DOTA peptide ChL6 in nude mice with human breast tumors (HBT) and ^{90}Y DOTA peptide H170 in nude mice with MCF-7 tumors. Potential enhancement of radioimmunotherapy by low dose tamoxifen, and peptides blocking other growth receptors, will be evaluated in these breast cancer models and correlated to mRNA expression of genes listed above. The methodology for the tumor genetic expression panel was developed under current funding and each selection has been shown to have a relationship to radiation or hormone triggered programmed cell death or patient prognosis (43-45). We will compare patterns of tumor response to variations in these mRNA levels. It is hoped that exploration of molecular mechanisms related to tumor cell death can lead to future studies of combined agents from which can determine synergistic triggers for programmed cell death in tumor cells.

During the past two years, we have refined our quantitative RNA/PCR assay. Samples are run in triplicate PCR reactions for each gene analyzed and dot blotted with subsequent nonisotopic probing. Adapting to the dot blot allowed us to reduce variability to 14%. An examination of human cancers for expression of the *NM23* family (*NM23-H1* and *-H2*) revealed a significant decrease in *NM23-H2* as cancer stage increased. This manuscript has been submitted. We have also studied levels of *MDR-1* expression in human tumors using this

approach (125).

Human Dosimetry and Therapeutic Human Use Radiopharmaceuticals

MoAb radiopharmaceuticals prepared for dosimetry or therapeutic feasibility (human use) during this period of report are presented in the following Table.

TABLE 3

	Imaging		Therapy	
Radiopharmaceutical	Doses	mCi	Doses	mCi
^{67}Cu-2IT-BAT-Lym-1	12	98	8	689
^{111}In-2IT-BAD-Lym-1	5	24	NA	NA

NA Not applicable.

Numerous *in vivo* experiments were also conducted in both tumored and non-tumored nude mouse models. Biodistribution studies were conducted in both tumored and non-tumored mice for the assessment of chemical stability, *in vivo* kinetics and processing (metabolism/catabolism) and toxicity of the radiopharmaceuticals. Other studies were carried out in tumor models with the objectives of simulating therapy and obtaining information on the therapeutic enhancement mechanisms. A summary list of all the animal study preparations is presented in the following Table.

TABLE 4

MoAb radiopharmaceutical preparations for mouse biodistribution, toxicity, therapy and autoradiography studies during the current funding period.

Radiopharmaceutical	Biodistribution uCi	Therapy uCi	Autoradiography uCi
^{125}I-Lym-1	3084	-	616
^{111}In-2IT-BABE-Lym-1	272	–	–
^{111}In-Pep-DOTA-Lym-1	272	–	–
^{111}In-2IT-BAD-Lym-1	903	–	–
^{90}Y-2IT-BAD-Lym-1	–	450	–
^{90}Y-Pep-DOTA-Lym-1	175	–	1100
^{67}Cu-2IT-BAD-Lym-1	80	–	–
^{125}I-mL-6	3821	–	–
^{111}In-CITC-Br96	150	20379	–
^{67}Cu-2IT-BAT-Br96	–	168	1000
^{111}In-2IT-BAT-ChL6	1452	–	550
^{111}In-Pep-DOTA-ChL6	1200	–	–
^{88}Y-2IT-BAD-ChL6	85	–	2266
^{90}Y-2IT-BAD-ChL6	745	–	–
^{90}Y-Pep-DOTA-ChL6	765	–	–
^{90}Y-2IT-BAD-BrE-3	–	11600	70
^{90}Y-MX-DTPA-BrE-3	700	8300	300

Information generated by animal experiments with these radiopharmaceuticals has been used in planning our clinical dosimetric/biokinetic and therapy feasibility/toxicity protocols. Some studies have also been published (126-131).

STUDIES IN PHANTOMS

Planar Image Quantitation. A primary concern for this project is to continuously improve the quantitative planar imaging methods used by our group. During this past grant period studies included validation of image quantitation methods in organs and tumors. Coincidence correction and quantitation of ^{90}Y using bremsstrahlung imaging were also studied.

Counts Coincidence Correction. Due to counts coincidence, significant errors have been found in image counts over the therapeutic range of ^{131}I and ^{67}Cu. At an injected dose level of 100 mCi of ^{67}Cu in the patient, the total observed count rate by the dual detector camera (Siemens Bodyscan) reached a maximum of 140K counts per second. The count loss in an image of the chest or abdomen was over 70 % of the true counts. Methods have been explored to correct planar gamma camera static images of an abdominal phantom for the resolving time errors encountered with the gamma camera. A simple method was evaluated in which a 10 ml reference source containing about 200 μCi was imaged in the same field of view of each patient image. The number of counts from the reference source was expressed

as a ratio of the counts detected from an image of the source in air alone to the counts from the reference source in the patient image to determine the count loss for each frame. Errors in correction may occur when the photopeak shape and position are not preserved using this method. Validation of this reference source method on the Siemens gamma camera was performed using ^{67}Cu concentrations similar to those of therapy doses in a phantom. The quantitation errors of this correction method were reasonably small. At an injected dose level of about 100 mCi of ^{67}Cu, the count loss in an abdominal image was estimated to be greater than 70 % of the actual counts. This loss of counts was corrected with an accuracy within 15 % using this simple correction method.

Organ Studies. In order to provide a basis for radiation dosimetry in planning targeted molecular therapy, it was necessary to validate the quantitative methods used. Planar imaging methods for quantitating ^{123}I, ^{99m}Tc, and ^{111}In in the liver and spleen of the abdominal phantom were assessed using a gamma camera. In the first approach, the number of counts detected in a single image of the liver or spleen was used to measure radionuclide content using an attenuation correction factor (ACF) calculated from data obtained without radioactivity in the background volume of the phantom. In two other methods, radionuclide content was derived from either the geometric mean (GM) of counts in conjugate images or in individual, opposed pixels of the conjugate images. The influence of background counts on quantitation was studied by adding a measured concentration of radioactivity to the background cavity of the abdominal phantom. The best estimates of radionuclide content were obtained by quantitation from the GM of counts in conjugate images of the liver and spleen. Radionuclide content of the liver and spleen could be determined from a single image if an appropriate correction for attenuation was available. These results provided a basis for radiation dosimetry for these and similar organs in patients.

Tumor Studies. Determination of the actual dose to tumors is important in evaluating the efficacy of a radiolabeled molecular construct. Accurate planar quantitation for tumors is made difficult by their relatively small size and radionuclide content when compared to surrounding larger organs and high background activity found in tissues. Limited studies on planar quantitation of ^{131}I in tumors have been previously reported. Quantitation of the size and amount of uptake of ^{131}I in tumors was investigated in order to obtain the best threshold with variation in activity concentration, source size, tumor depth and background activity using an Alderson abdominal phantom (132). Better quantitative accuracy was established when a deeply seated tumor was quantified using the geometric-mean of conjugate view method and when a superficial tumor was quantified using the effective point source method. The accuracy of estimation of radionuclide amount was within 10 % for 3-5 cm tumors and was better than 20 % for a 1 cm tumor at all tumor and background concentrations and locations in the phantom.

^{90}Y Quantitation With Bremsstrahlung Imaging. Studies of ^{90}Y quantitation using bremsstrahlung imaging have been conducted to predict the behavior of ^{90}Y in-vivo. Conventional gamma photon imaging methods cannot be simply applied to imaging of the bremsstrahlung continuous energy spectrum. The spatial and energy dependence of bremsstrahlung production cause an inherent limitation in spatial resolution for bremsstrahlung imaging. While high energy photons are created near the decay site, most low energy bremsstrahlung photons are produced farther from the ^{90}Y decay location (133). On the other hand, degradation of the bremsstrahlung image is, in part, due to septal penetration from high energy photons of the continuous energy spectrum from ^{90}Y decay. These photons are accepted in the selected energy window as Compton scattered events in the camera crystal. The energy distribution of Compton photons within the selected energy window influences image resolution. The choice of collimation and energy window represents

a practical compromise between sensitivity and spatial resolution requirements for specific circumstances. The detector system sensitivity, resolution and image S/N were investigated for various collimators and energy windows. Studies on accuracy of quantitation of ^{90}Y activity in an Alderson abdominal phantom have also been performed using the geometric mean of conjugate view or effective point source methods (134). To overcome problems of unclear visual boundaries inherent to imaging of bremsstrahlung a contrast recovery method was developed. Methods of quantitative bremsstrahlung imaging have been enhanced by the use of a Wiener filter to deconvolve the septal penetration and scatter (Figure 9).

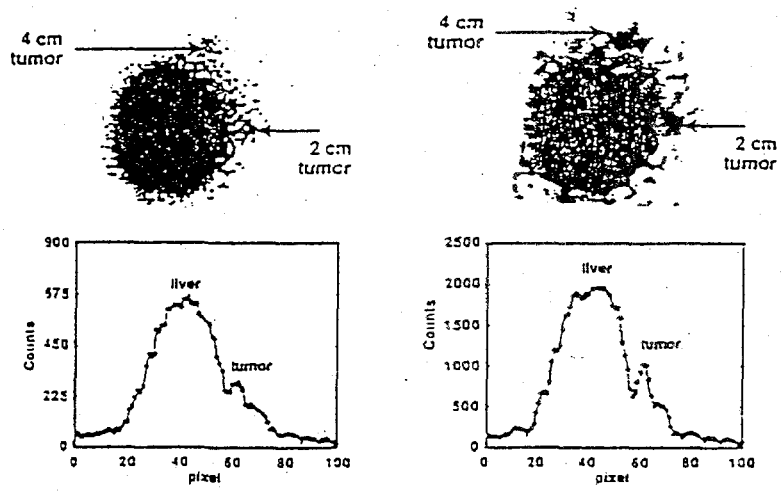

Figure 9.

Comparison of anterior phantom images and line profiles before (left) and after (right) Wiener filtering. Tumor definition was enhanced on the images (top left and right) as shown by the difference in the line profiles (bottom left and right).

A three-fold improvement in resolution recovery was achieved for full width at tenth maximum of a ^{90}Y line source when placed in 10 cm of water. Tumor definition was facilitated after Wiener filtering. Tumor and organ quantitation on filtered images in a phantom study yielded an estimation accuracy of better than 10 % for cumulated activity in the liver, spleen and 4 cm tumor. These results were comparable to those obtained from a single photon emitter such as ^{131}I using planar imaging (135).

QUANTITATIVE SPECT

The intrinsic difficulty in planar quantitation is background subtraction when organs are superimposed. SPECT effectively eliminates the problems of superimposition of organs and tissues and improves target to non-target image contrast. SPECT has the potential to quantify radionuclide and mass with greater accuracy in comparison to planar imaging. Practical SPECT measurement of radionuclide content requires: 1) accurate determination of camera sensitivity; 2) accurate definition of region of interest to determine the number of counts within it; 3) correction for attenuation; 4) correction for scatter and septal penetration; 5) accurate measurement of the administered dose; 6) adequate statistics; and 7) accurate definition of tissue mass or volume (136). We have made substantial progress in dealing with these issues especially in the areas of photon attenuation and scatter correction.

Attenuation Correction. Quantitative tomography must address the requirement for accurate boundary determination in each transverse section and greater sensitivity to errors in the attenuation correction. First, we have investigated improved methods of boundary definition for attenuation correction in SPECT. Three Compton scatter methods have been investigated using a source of ^{99m}Tc (137). The 90-degree Compton scatter method was found to give the best boundary definition. This method entails the use of a source (that does not superimpose any part of the patient or phantom) placed 90 degrees to the front of the detector. We have also investigated a modified post processing correction matrix for photon attenuation correction (138). When the transverse section images were corrected for attenuation the liver and spleen were similarly elevated by the same scatter fraction. The post reconstruction correction matrix generated with the narrow beam linear attenuation coefficient value of 0.15/cm for the 140 keV photons emitted by the ^{99m}Tc calibration source was used in this method. When this correction was applied to the phantom sources, the radionuclide content of the liver and spleen was determined with better than 10 % accuracy.

Scatter Correction. One of the principal obstacles in the use of SPECT for absolute quantitation has been the inclusion of a large fraction of the counts that arise from scatter detected in a region of interest that outline the boundary of an organ on a transverse section image provided by SPECT. The scattered events that originate from the source activity are added to scatter from all other sources that are inside and outside any particular transverse section both inside and outside the direct field of view of the camera. Since Jaszczak (68) proposed a method to estimate the scatter events using counts in a scatter window, scatter subtraction has received a lot of attention because of its effectiveness and practicality. Because the scatter events in the energy window is also related to the photons emitted from higher energies (eg. ^{131}I 637 keV scatter to 364 keV window, ^{67}Cu 184 keV scatter to 93 keV window), it is more reasonable to estimate scatter events using a dual scatter window above and below the photopeak.

Because of the high energy and significant septal penetration with ^{131}I, correction factors must be determined that are unique to this radionuclide. A primary energy window of 15 % centered at 364 keV was selected for the primary photopeak. Two scatter windows above and below the primary energy window were used for collecting scatter photons. The image from the scatter window was subtracted from the primary photopeak image before reconstruction of the images was done, and Chang's attenuation correction method (67) was subsequently applied. With this scatter subtraction method, we were able to quantify activity in the liver phantom as well as volumes of both the liver and spleen with better than 10 % accuracy. We also estimated volumes with an accuracy better than 90 %.

Accurate quantitation of ^{67}Cu is also necessary to depict the biodistribution of these radiolabeled targeted molecules in patients. While the primary photon emission energies of ^{67}Cu at 93 keV and 184 keV are more suitable for imaging than those of ^{131}I, its dual photopeaks raise issues in quantitative imaging different from other radionuclides. Scatter subtraction was performed on projection data using measured "k" scatter values for the 92 keV, 184 keV energy windows and for a combination window around each of the 92 and 184 keV photopeaks. Attenuation correction was performed with the linear attenuation coefficient measured from either a rod transmission scan or transmission fraction data from a small volume source in water. We found that image quality or quantitation results obtained using the 184 keV energy window were generally better than with either the 92 keV or combined 92 and 184 keV energy windows. However for a single detector SPECT system, the combination window should be utilized when counts are low e.g. for acquisition times of less 45 minutes when the remaining activity in the patient is less than 4 mCi.

PRECLINICAL STUDIES

The goal of performing preclinical studies is to provide experimental models of human disease in mice to optimize molecular targeting and therapy for cancer. First, quantitation information on organ and tumor uptake of targeted molecules provides basic criteria for evaluating therapeutic efficacy and toxicity. Whole body autoradiography has been shown to be a powerful tool in quantitation of uptake of radioactivity. Second, previous studies demonstrated that the effectiveness of radiolabeled targeted molecular therapy depends on a number of factors relating to the targeted molecule such as specificity, affinity, and immunoreactivity (139). The density, location, and heterogeneity of molecular distribution within tumors have significant effects on therapeutic efficacy. One of the obstacles for cancer therapy with radiolabeled targeted molecules is the problem of tumor penetration. The effectiveness of cancer cell killing is hindered by heterogeneity of the radiation dose in tumor. The study of this heterogeneous radiation dose is observed by imaging. Spatial resolution of SPECT is in the order of several millimeters and therefore is limited to yielding information at macroscopic levels. Autoradiography provides a good opportunity for evaluating molecular biodistribution at a tissue level. The information obtained from autoradiography is fundamental to understanding and improving the behavior of these molecules in tumors and normal tissues.

We have investigated uptake of ^{90}Y-BrE-3 in mice using autoradiography. ^{90}Y is a promising therapeutic radionuclide and reduces the problem of dose heterogeneity in small tumors because of its long range beta emission. Radiation dose to the tumors in mice was anticipated to be uniform. However, therapeutic trials demonstrated escape of ^{90}Y from radiolabeled molecules and uptake by the skeleton with resultant bone marrow toxicity. We attempted to evaluate the importance of this factor by a comparison of the radiation dose to the marrow when chelated by either of two high affinity chelators, MX-DTPA or BAD. Quantitative autoradiography revealed substantially greater uptake of ^{90}Y in the skeleton when MX-DTPA was used as the chelator. These observations suggested that ^{90}Y escape to bone was a significant factor in the maximum tolerated dose of radiolabeled targeted molecule that can be used in therapeutic trials. Meanwhile, results of tumor imaging with autoradiography confirmed a uniform radiation dose distribution of ^{90}Y in mice for both chelators (140).

CLINICAL STUDIES

The objective of quantitative imaging is to provide information on molecular behavior in patients that is analogous to that provided by biodistribution studies in mice. The amount of radionuclide in a specific site can be estimated by relating the counts detected in a defined region of interest to the total radionuclide content. The reliability of evaluations using quantitative imaging have been further investigated by correlating image quantitation with counts of biopsy samples and deriving S factors for tumor and organ radiation dose calculation. Images of patients who had received intravenous targeted molecules labeled with ^{111}In, ^{67}Cu or ^{131}I were obtained and quantitations performed by previously described methods (141,142). Using the techniques described, we were able to study dynamic molecular biodistributions and evaluate efficacy and toxicity of various molecular constructs and radionuclides.

Image Quantitation verses Counts From Biopsy Samples. To further assess the accuracy of image quantitation in-vivo, we have compared tumor quantitation results from imaging methods with biopsy counting methods. A correlation was found between the concentration

of radionuclide observed by counting tumor biopsy samples and that observed by quantitative imaging (Figure 10).

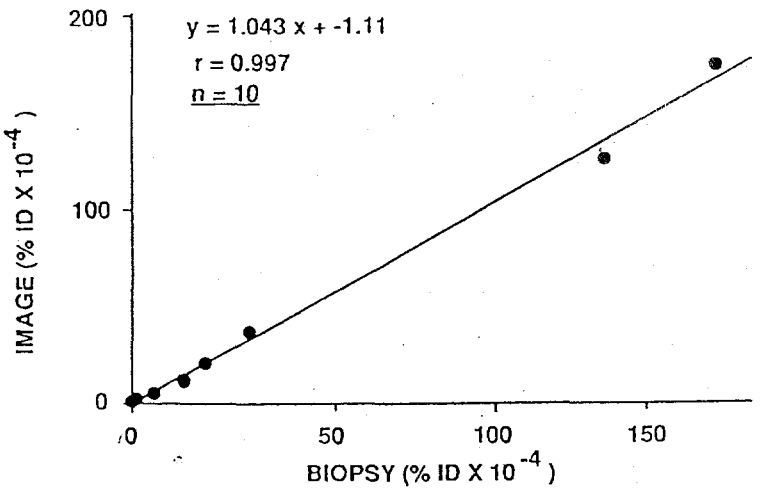

Figure 10.
Correlation of tumor concentration of I-131 Lym-1 determined by counting biopsy sample and imaging patient.

S Factors For Radiation Dose Calculation. Studies have been carried out to identify possible sources of error in radiation dose estimation apart from activity quantitation. The influence of remaining body activity on the calculated radiation absorbed doses delivered to various organs or tumor sites in the body has been investigated for patients receiving diagnostic and therapy doses of ^{131}I labeled Lym-1 considering the liver as both the target and the source. Good agreement was found using the corrected cumulated activity and the corrected S factor methods. Doses were overestimated by up to 20% for the liver using the straightforward MIRD approach. This correction factor was small for typical tumor sites of less than 100 ml with uptake of less than 1% of the administered dose. The remaining body activity correction factor can be elegantly calculated for any site in the body from a whole body image and a static image of a specific site.

Currently available MIRD tables have been commonly used for calculation of radiation dosimetry for tumors up to 100 grams (143). However, it is not uncommon to find tumor mass greater than 100 grams in clinical studies. Methods need to be developed to derive S factors for larger tumors. We have evaluated simple interpolation methods to estimate S factors for various tumors by interpolation of S factors of normal organs in the MIRD table. Because of the relatively small amounts of contribution from penetrating radiations (for ^{67}Cu and ^{131}I), simple interpolation of S factors is possible with reasonable accuracy. The quantitative difference between tumor S factors derived from the interpolation method and those derived by the method of Ellett & Humes (143) is less than 7 %. These results encouraged us to extend this work in future studies for deriving S factors for organs in individual patients using simple interpolation methods.

^{67}Cu Imaging Studies For Lymphoma Cancer. Imaging is used to evaluate novel radiolabeled targeted molecules in the ultimate biologic system, i.e. patients. While ^{131}I is a practical radionuclide, it is not ideal for targeted molecular therapy because of dehalogenation and substantial imaging and radiation safety problems secondary to multiple energetic photons.

^{67}Cu has been advocated for targeted molecular therapy because of its superior physical characteristics and observations that its retention in tumors when conjugated to targeted molecules was longer than that of the corresponding radioiodinated targeted molecule leading to an increased radiation absorbed dose to the tumor. Quantitative imaging was used to explore the use of ^{67}Cu as therapeutic radionuclides for targeted molecular therapy.

The efficiencies of our scintillation cameras were about four times greater for ^{67}Cu than for ^{131}I despite the lesser abundance of ^{67}Cu photons. This relates to the fact that the photons of ^{67}Cu are ^{99m}Tc-like in energy and more efficient for a scintillation camera than the more energetic photons of ^{131}I. For the same amount of radioactivity and number of counts, superb images were obtained four times faster after injection of ^{67}Cu-BAT-Lym-1 than after injection of ^{131}I Lym-1. The quality and resolution of the ^{67}Cu images were superior to those obtained with ^{131}I (Figure 11).

Figure 11.

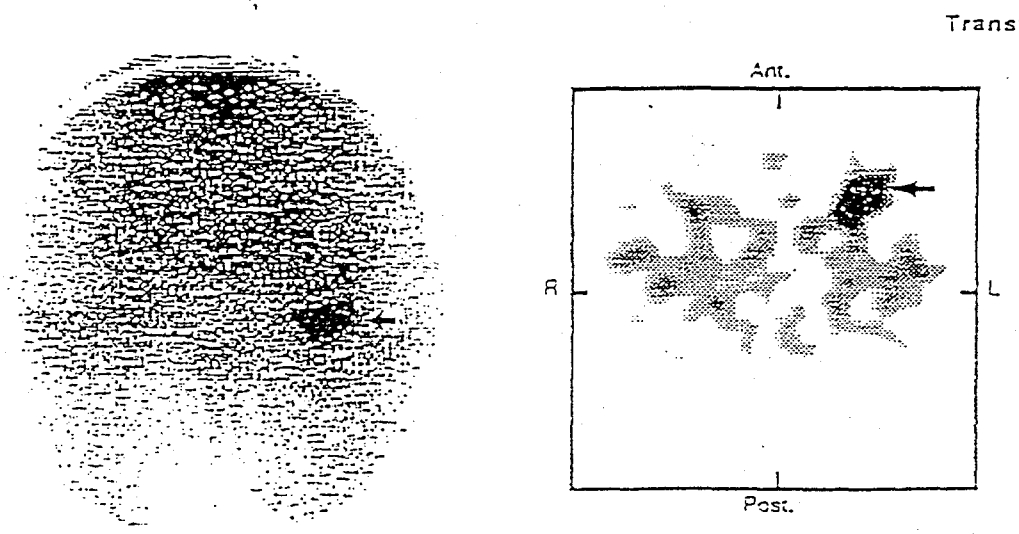

Retention of ^{67}Cu by the liver was longer than that of ^{131}I leading to a modestly greater radiation absorbed dose to the liver which is not a dose limiting organ (Table 5).

TABLE 5.

Radiation Dosimetry for ^{67}Cu-2IT-BAT-Lym-1

	Radiation Dose (rads/mCi)
Whole Body	0.38-0.49
Liver	4.26-9.01
Spleen*	3.08-12.6
Kidney	0.93-3.1
Marrow**	0.15-0.47
Tumor***	0.2-51.0
Lung	0.58-2.46

*diseased
**from blood and body
***1.4-5.4 X greater than ^{131}I Lym-1

Targeted molecular imaging allowed us to compare the dosimetry for ^{67}Cu-2IT-BAT-Lym-1 with that for ^{131}I Lym-1. In all instances, the radiation absorbed dose to the tumors was 1.4-5.4 times greater for ^{67}Cu than for ^{131}I because the ^{67}Cu was retained in the tumors much longer than was ^{131}I. Patients that received ^{67}Cu-2IT-BAT-Lym-1 had significant decreases in the size of their tumors after administration of the antibody.

^{111}In MoAb Imaging Studies For Breast Cancer to Predict ^{90}Y MoAb Therapy. ^{90}Y is another radionuclide bound to novel molecular constructs that has been investigated by imaging. ^{90}Y has attracted considerable attention for targeted molecular therapy because its physical properties decrease radiation safety concerns and avoid the requirement for hospitalization. Its long range beta emission reduces the problem of tumor penetration. Furthermore, radiometal immunoconjugates, such as those of ^{90}Y, have longer residence times in malignant tissues than equivalent iodinated immunoconjugates, albeit, this is often true for normal tissues as well. These considerations contributed to development of molecular probes attached to ^{90}Y and the use of these ^{90}Y molecular agents in clinical trials of targeted molecular therapy, such as BrE-3, an anti-breast cancer MoAb formulated with MX-DTPA. Because ^{90}Y lacks gamma emissions for imaging studies, ^{111}In labeled antibody has been co-administered since its chemical behavior is analogous to that of ^{90}Y.

Patient imaging studies demonstrated excellent tumor uptake for this anti-breast cancer molecular probe (Figure 12).

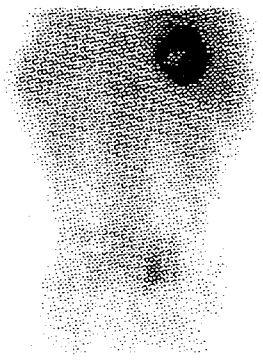

Figure 12.

The advantage of ^{90}Y over ^{131}I can be easily illustrated, for example, as we compare tumor radiation dose for a MoAb targeted to breast cancer, ChL6, labeled with ^{90}Y and ^{131}I. Uptake of ^{131}I-ChL6 observed in tumors of patients in clinical trials has ranged from 0.1 to 0.001% ID/gm. Using this range of uptake for ^{131}I ChL6 and for ^{90}Y DOTA ChL6 and the biological data observed for human adenocarcinoma tumors in nude mice for ^{131}I ChL6 and for ^{90}Y ChL6, the following table was generated using conventional methods and confirms the enhanced radiation to the tumor that can be expected when ^{90}Y is used for therapy (Table 6).

TABLE 6.

RAD DOSE TO TUMOR ($^{131}I/^{90}Y$) per mCi

Tumor Size	0.1% ID/gm		0.01 % ID/gm		0.001% ID/gm	
	^{131}I	^{90}Y	^{131}I	^{90}Y	^{131}I	^{90}Y
10 gm	62.1/241		6.21/24.1		0.621/2.41	
50 gm	64.6/241		6.46/24.1		0.646/2.41	
100 gm	67.6/241		6.76/24.1		0.676/2.41	

DOE Cited Publications

1994 Kukis, D.L., H. Diril, D.P. Greiner, S.J. DeNardo, G.L. DeNardo, C.F. Meares. A comparative study of Copper-67 radiolabeling and kinetic stabilities of antibody-macrocycle chelate conjugates. Cancer (suppl) 73:779-786.

1994 DeNardo, G.L., L.A. Kroger, S.J. DeNardo, L.A. Miers, Q. Salako, D.L. Kukis, I. Fand, S. Shen, O. Renn, C.F. Meares. Comparative toxicity studies of yttrium-90 MX-DTPA and 2-IT-BAD conjugated monoclonal antibody (BrE-3). Cancer (suppl) 73:1012-1022.

1994 DeNardo, S.J., G.R. Mirick, L.A. Kroger, L.F. O'Grady, K.L. Erickson, I. Hellstrom, K.E. Hellstrom, G.L. DeNardo. The biologic window for ChL6 radioimmunotherapy. Cancer (suppl) 73:1023-1032.

1994 DeNardo, G.L., S.J. DeNardo, D.J. Macey, S. Shen, L.A. Kroger. Overview of radiation myelotoxicity secondary to radioimmunotherapy using ^{131}I-Lym-1 as a model. Cancer (suppl) 73:1038-1048.

1994 DeNardo, G.L., J.P. Lewis, S.J. DeNardo, L.F. O'Grady. Effect of Lym-1 radioimmuno-conjugate on refractory chronic lymphocytic leukemia. Cancer 73:1425-1432.

1994 Shen, S., G.L. DeNardo, A Yuan, D.A. DeNardo, S.J. DeNardo. Planar gamma camera imaging and quantitation of yttrium-90 bremsstrahlung. Journal of Nuclear Medicine, 35:1381-1389.

1994 DeNardo, S.J., L.F. O'Grady, C.M. Richman, G.L. DeNardo. Overview of radioimmunotherapy in advanced breast cancer using I-131 Chimeric L6. In RL Ceriani (Ed.), Antigen and Antibody Molecular Engineering in Breast Cancer Diagnosis, Plenum Press, New York, pp 203-211.

1994 Shen, S., G.L. DeNardo, S.J. DeNardo. Quantitative bremsstrahlung imaging of yttrium-90 using a Wiener filter. Medical Physics 21:1409-1417.

1994 DeNardo, G.L., S.J. DeNardo. Overview of obstacles and opportunities for radioimmunotherapy of cancer. In DM Goldenberg (Ed.), Cancer Therapy with Radiolabeled Antibodies, CRC Press, Boca Raton, Florida, pp 141-154.

1994 DeNardo, G.L., S.J. DeNardo. Treatment of B-lymphocyte malignancies with ^{131}I-Lym-1 and ^{67}Cu-2IT-BAT-Lym-1 and opportunities for improvement. In DM Goldenberg (Ed.), Cancer Therapy with Radiolabeled Antibodies, CRC Press, Boca Raton, Florida, pp 217-227.

1994 DeNardo, G.L., K.R. Lamborn, S.J. DeNardo, L.A. Kroger. Use of response surface statistical designs to detect effects of biologic response modifiers such as IL-2. Biotechnology Therapeutics 5(1&2):15-26.

1995 Macey, D.J., S.J. DeNardo, G.L. DeNardo, D.A. DeNardo, S. Shen. Estimation of radiation absorbed doses to the red marrow in radioimmunotherapy Clinical Nuclear Medicine 20(2):117-125.

1995 Kukis, D.L., G.L. DeNardo, S.J. DeNardo, G.R. Mirick, L.A. Miers, D.P. Greiner, C.F. Meares. Effect of the extent of chelate substitution on the immunoreactivity and biodistribution of 2IT-BAT-Lym-1 immunoconjugates Cancer Research 55:878-884.

1995 DeNardo, G.L., S.L. Mills, D.L. Kukis, V. Anderson, S.J. DeNardo. Review of a four-year experience iodinating monoclonal antibodies with therapeutic amounts of I-131. Antibody, Immunoconjugates, and Radiopharmaceuticals 8:1-10.

1995 DeNardo, S.J., G-R. Zhong, Q. Salako, M. Li, G.L. DeNardo, C.F. Meares. Pharmacokinetics of chimeric L6 conjugated to ^{111}In- and ^{90}Y-DOTA-peptide in tumor bearing mice. Journal of Nuclear Medicine 36:829-836.

1995 Lewis, J.P., G.L. DeNardo, S.J. DeNardo. Radioimmunotherapy of lymphoma: A UC Davis experience. Hybridoma 14(2):115-120.

1995 DeNardo, G.L., L.A. Kroger, G.R. Mirick, K.R. Lamborn, S.J. DeNardo. Analysis of antiglobulin (HAMA) response in a group of patients with B-lymphocyte malignancies treated with ^{131}I-Lym-1 International Journal of Biological Markers. 10(2):67-74.

1995 DeNardo, G.L, K.R. Lamborn, S.J. DeNardo, D.S. Goldstein, E.G. Dolber-Smith, L.A. Kroger, E.C. Larkin, S. Shen. Prognostic factors for radioimmunotherapy in patients with B-lymphocytic malignancies. Cancer Research (Suppl.) 55:5893s-5898s.

1995 DeNardo, S.J., P.H. Gumerlock, M.D. Winthrop, P.C. Mack, S-G. Chi, K.R. Lamborn, S. Shen, L.A. Miers, R.W deVere White, G.L. DeNardo. Yttrium-90 chimeric L6 therapy of human breast cancer in nude mice and apoptosis related mRNA expression. Cancer Research (Suppl.) 55:5837s-5841s.

1995 Wilder, R.B., J.F. Fowler, G.L. DeNardo, S. Shen, B.W. Wessels, S.J. DeNardo. Use of the linear-quadratic model to compare doses delivered to the bone marrow by fractionated ^{131}I-Lym-1 radioimmunotherapy. Antibody, Immunoconjugates, and Radiopharmaceuticals 8(4):227-239.